UCLA
UCLA Previously Published Works

Title
Experimental and Theoretical Exploration of the Kinetics and Thermodynamics of the Nucleophile-Induced Fragmentation of Ylidenenorbornadiene Carboxylates.

Permalink

Journal
Journal of Organic Chemistry, 88(16)

Authors
Richardson, Abigail
LHeureux, Scott
Henry, Ava
et al.

Publication Date
2023-08-18

DOI
10.1021/acs.joc.3c00980

Peer reviewed

Experimental and Theoretical Exploration of the Kinetics and Thermodynamics of the Nucleophile-Induced Fragmentation of Ylidenenorbornadiene Carboxylates

Abigail D. Richardson, Scott J. L'Heureux, Ava M. Henry, Elizabeth A. McDonough,
Cameron J. Fleischer, Cameron C. McMullen, Trevor R. Reynafarje, Gisele P. Guerrero,
Quinn E. Williams, Qingyang Zhou, David M. Malouf, Spencer E. Thurman, Julia E. Soeller,
Jerry Y. Sheng, Erica A. Medhurst, Angel E. Canales, Ty B. Cecil, K. N. Houk, Philip J. Costanzo,
and Daniel A. Bercovici*
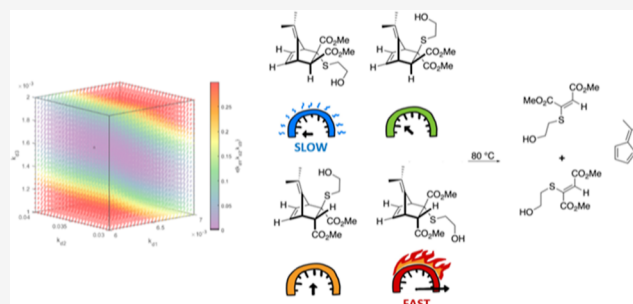
ACCESS | 📊 Metrics & More | 📖 Article Recommendations | 🆂�ᴵ Supporting Information

ABSTRACT: Ylidenenorbornadienes (YNDs), prepared by [4 + 2] cycloadditions between fulvenes and acetylene carboxylates, react with thiol nucleophiles to yield mixtures of four to eight diastereomers depending on the symmetry of the YND substrate. The mixtures of diastereomers fragment via a retro-[4 + 2] cycloaddition with a large variation in rate, with half-lives ranging from 16 to 11,000 min at 80 °C. The diastereomer-enriched samples of propane thiol adducts [YND-propanethiol (PTs)] were isolated and identified by nuclear Overhauser effect spectroscopy (NOESY) correlations. Simulated kinetics were used to extrapolate the rate constants of individual diastereomers from the observed rate data, and it correlated well with rate constants measured directly and from isolated diastereomer-enriched samples. The individual diastereomers of a model system fragment at differing rates with half-lives ranging from 5 to 44 min in CDCl₃. Density functional theory calculations were performed to investigate the mechanism of fragmentation and support an asynchronous retro-[4 + 2] cycloaddition transition state. The computations generally correlated well with the observed free energies of activation for four diastereomers of the model system as a whole, within 2.6 kcal/mol. However, the observed order of the fragmentation rates across the set of diastereomers deviated from the computational results. YNDs display wide variability in the rate of fragmentation, dependent on the stereoelectronics of the ylidene substituents. A Hammett study showed that the electron-rich aromatic rings attached to the ylidene bridge increase the fragmentation rate, while electron-deficient systems slow fragmentation rates.

INTRODUCTION

Transformations known to the chemistry community as "click" reactions have become immensely popular methods in many fields of chemistry for their ability to covalently bond two components in a modular and facile manner.[1] The 2022 Nobel prize in chemistry, which was awarded to Sharpless, Meldal, and Bertozzi for their pioneering work in "click" chemistry and its applications, highlights the breadth and utility of this class of reactions.[2] "Clip" reactions, as their name suggests, conversely offer the capability to break covalent bonds in a similarly facile and modular manner. A recent review by Johnson and co-workers divides "clip" reactions into six main classifications: stoichiometric, catalytic, electron-transfer-mediated, light-mediated, thermally mediated, and force-mediated.[3] A list of commonly utilized "click" and "clip" reactions is given in Scheme 1. It is of interest to note that [4 + 2] cycloadditions and their retrograde reactions (retro-[4 + 2]) are able to react as both "click" and "clip" reactions, respectively. We previously

utilized these reactions as dynamic covalent linkages to understand and manipulate polymer topology and solubility.[4−9] Seminal work by the Finn group has shown that furans can react via [4 + 2] cycloadditions with alkyl acetylenedicarbonyls to yield oxanorbornadienes (ONDs), which can be fragmented via a retro-[4 + 2] cycloaddition after conjugate addition of an appropriate nucleophile.[10−14] The furan component is thus "clicked" on to an alkyl acetylenedicarboxylate and subsequently "clipped" off again after reaction with the nucleophile, as depicted in Scheme 2. These OND "click-

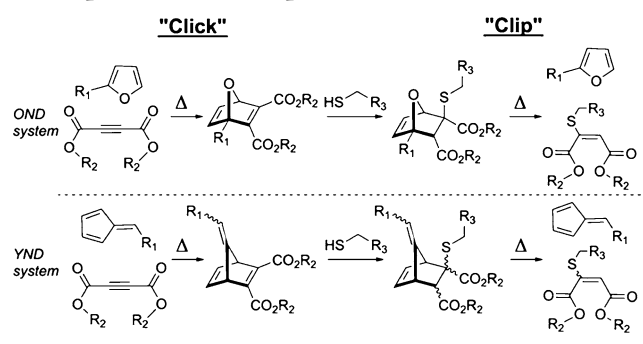## Scheme 1. Various "Click" and "Clip" Reactions
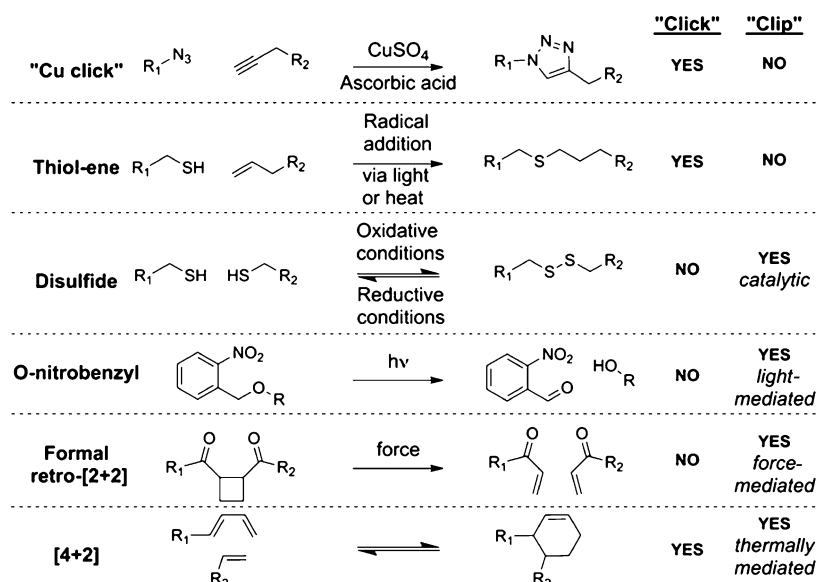
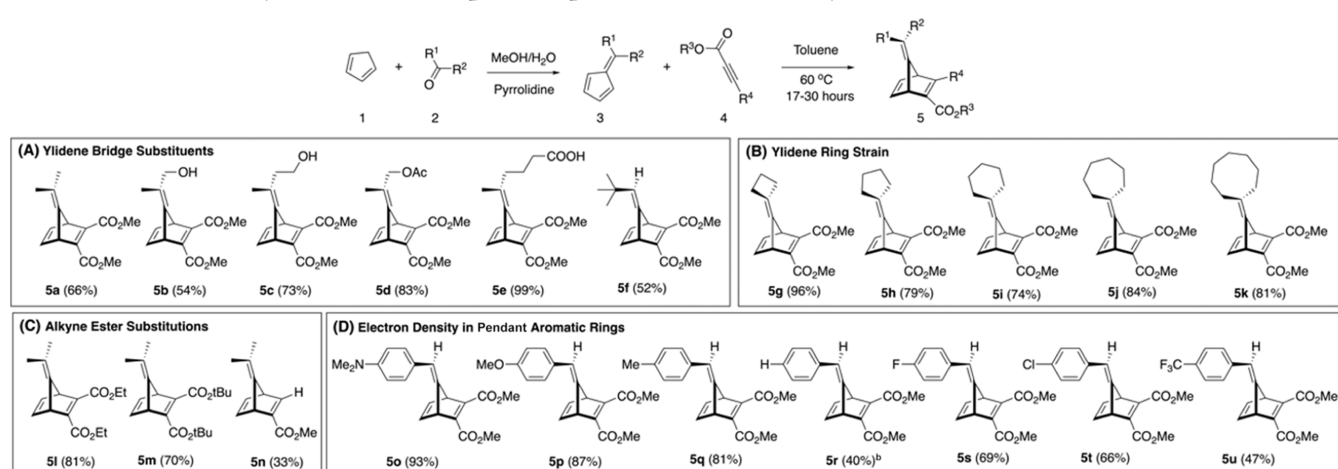## Scheme 2. OND and YND Systems as "Click" and Nucleophile-Induced "Clip" Reactions

and-clip" systems have already shown utility as fluorogenic probes,[10,15] pharmaceutical delivery systems,[13,16–18] linkages in degradable hydrogels,[19,20] and scaffolds toward the synthesis of difficult-to-prepare substituted heterocycles.[21,22] We have further built on this "click-and-clip" strategy by reacting

fulvene substrates in the place of furans with alkyl acetylenedicarboxylates to yield ylidenenorbornadienes (YNDs).[23]

Unlike their OND counterparts, YND substrates reacted with a thiol nucleophile, beta-mercaptoethanol (BME), to provide a complex mixture of diastereomers. These diastereomers subsequently showed marked differences in the fragmentation "clip" reaction rates. Herein, we build upon the scope of YND substrates as "click-and-clip" systems and describe our experimental and theoretical exploration into the kinetics and mechanism of fragmentation of YND-thiol diastereomer adducts.

■ RESULTS AND DISCUSSION

Synthesis of YNDs. Previously prepared YNDs (Scheme 3A,C—excluding **5e**), synthesized via [4 + 2] cycloadditions between fulvenes and acetylene carboxylates and dicarboxylates, provided yields from 33 to 83%. A new series of YNDs has been prepared (Scheme 3B,D) to further explore the scope and mechanism of the fragmentation. The yields of these
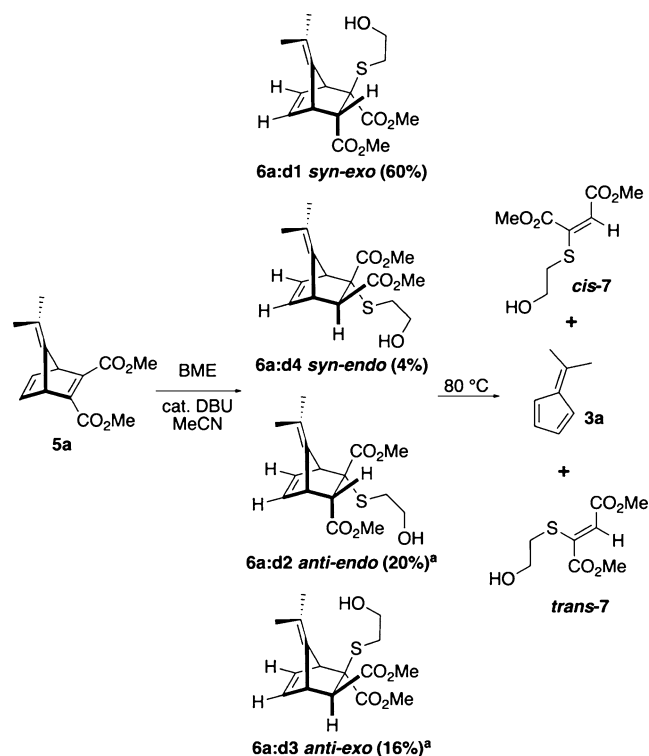
Scheme 3. YND Carboxylate Substrate Scope for Experimental Kinetic Analysis[a]

(A) Ylidene Bridge Substituents
5a (66%)   5b (54%)   5c (73%)   5d (83%)   5e (99%)   5f (52%)

(B) Ylidene Ring Strain
5g (96%)   5h (79%)   5i (74%)   5j (84%)   5k (81%)

(C) Alkyne Ester Substitutions
5l (81%)   5m (70%)   5n (33%)

(D) Electron Density in Pendant Aromatic Rings
5o (93%)   5p (87%)   5q (81%)   5r (40%)[b]   5s (69%)   5t (66%)   5u (47%)

[a]Asymmetric YNDs were recovered as a racemic mixture. [b]Yield taken over two steps from benzaldehyde.

YNDs were moderate to excellent (47−93%) with mild heating in toluene under an ambient atmosphere. 6-Aryl-substituted fulvenes generate YNDs in yields that trend up with increased electron density (Scheme 3D). Excellent yields were obtained from electron-rich phenyl rings (5o 93%), and yields decreased significantly with electron-poor phenyl rings (5u 47%). This result can likely be attributed to an increase in the favorability of competing fulvene dimerization via [4 + 2] cycloaddition, especially for electron-deficient fulvenes.[24] During chromatography of 5u, a fulvene dimer was observed as a minor side product.

Model System Kinetics. Nucleophile-induced fragmentation on the model YND system 5a was analyzed after conjugate addition with BME catalyzed by 1,8-diazabicyclo[5.4.0]undec-7-ene (DBU). The YND−BME adduct 6a displayed a complex mixture of four diastereomers 6a:d1-4, as seen in Scheme 4. As previously reported,[23] three

Scheme 4. Preparation and Fragmentation of YND−BME Diastereomers 6a:d1-4

6a:d1 *syn-exo* (60%)

6a:d4 *syn-endo* (4%)

6a:d2 *anti-endo* (20%)[a]

6a:d3 *anti-exo* (16%)[a]

cis-7

3a

trans-7

[a]As described later in this report, the assignment of diastereomers d2 and d3 has been reversed from our previous report.

diastereomers 6a:d1-d3 of the model system YND−BME provided overlapping signals in the ^{1}H NMR spectrum, and individual diastereomer rate constants could not be directly measured using DMSO-d_6 as the solvent. Diastereomer 6a:d4 did provide an isolated resonance in the ^{1}H NMR spectrum but was produced as only 4% of the total mixture, and relative to diastereomers 6a:d1-d3, 6a:d4 fragmented too slowly at 80 °C for accurate kinetic data to be obtained in the same experiment. Therefore, diastereomer 6a:d4 was not experimentally investigated further for fragmentation kinetic analysis. The integrated first-order rate plot resulting from the combination of degradation kinetics of diastereomers 6a:d1-d3 appeared curved (Figure S19), suggesting that

diastereomers were fragmenting at different rates. With the aid of kinetic simulations utilizing a genetic algorithm and the simplex method,[25] we were able to extrapolate the individual first-order rate constants from the observed convoluted data (Figure 1).

In an effort to validate the extrapolation method, we directly evaluated the kinetics of the fragmentation of individual diastereomers 6a:d1-d3 utilizing CDCl$_3$ as the solvent. In CDCl$_3$, the integration of individual diastereomer resonances resolved enough for the fragmentation kinetics to be measured directly by observing the disappearance of the individual signals assigned to diastereomers 6a:d1-3 (Figure S20). Kinetic simulations were then applied to extrapolate individual diastereomer fragmentation rate constants from the convoluted kinetics of the combined ^{1}H NMR integration values of diastereomers 6a:d1-d3. Comparison of these two methods (Table 1 and Figure 2) substantiated the use of the genetic algorithm and simplex method to adequately extrapolate the individual diastereomer kinetic rates from the convoluted kinetics of the complex mixtures. Extrapolated rate constants matched the directly measured rate constants fairly well for 6a:d1 and d2 as both the extrapolated values were within 20% of the directly measured values. The value for the 6a:d3 diastereomer was within 40%. We were unable to chromatographically separate the mixture of diastereomers for YND−BME 6a and thus could not directly measure individual rate constants in DMSO-d_6.

Substrate Scope. *Ylidene Bridge Substituent Kinetics.* Substituent effects were first explored through the modification of the functional groups atop the ylidene bridge (Table 2). As explained in our previous findings, a decrease in electron density at the ylidene bridge and changes in diastereomer populations affected the observed rates of the mixture of diastereomers.[23] Compared to the model system 6a ($t_{1/2}$ = 31.1 min), pendent alcohol substrates 6b ($t_{1/2}$ = 89.6 min) and 6c ($t_{1/2}$ = 53.2 min), and the acyl-substituted 6d fragmented at slower rates, with the most electron-deficient acyl-substituted 6d providing the longest half-life ($t_{1/2}$ = 226 min). Substrates 6b, 6d, and 6e ^{1}H NMR spectra allowed for the determination of diastereomeric ratios d1−d4 based on assignments from the model systems 6a and 8a (vide infra), suggesting that the E/Z stereocenter atop the ylidene bridge had little effect on the proton resonances used for diastereomer assignment. As such, when the extrapolation algorithm was applied to the observed kinetics of the mixture of diastereomers for substrates 6b, 6d, and 6e, the results (Table 2) confirmed that individually, all the extrapolated rate constants for diastereomers d1−d3 of these substrates decrease with electron-withdrawing ylidene bridge substituents. However, YND−BMEs 6c and 6f were recovered as a complex mixture of eight diastereomers that could not be resolved in the ^{1}H NMR spectra. Thus, our extrapolation technique could not be applied to compare individual diastereomer rate constants.
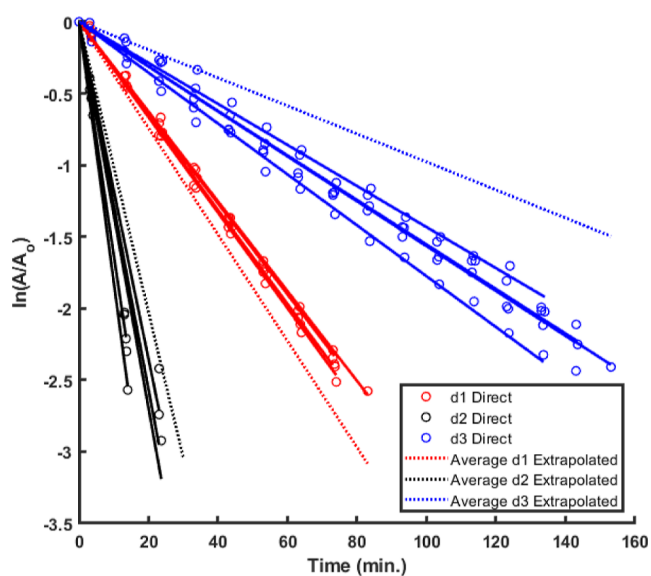
Ring Strain Kinetics. A near 50% drop in the observed half-life in YND−BME 6h ($t_{1/2}$ = 17.0 min) versus the model system 6a ($t_{1/2}$ = 31.1 min) was observed when the ylidene bridge was connected to a cyclopentane ring. It is well known that the increase in the carbonyl IR stretching frequency of cyclic ketones coincides with an increase in ring strain. This is largely a mechanical effect attributed to the change in C−C(= O)−C bond angle provided by the strain of the ring and not a large change in the C=O force constant.[26,27] This effect ultimately leads to the shortening of the C=O bond and thus
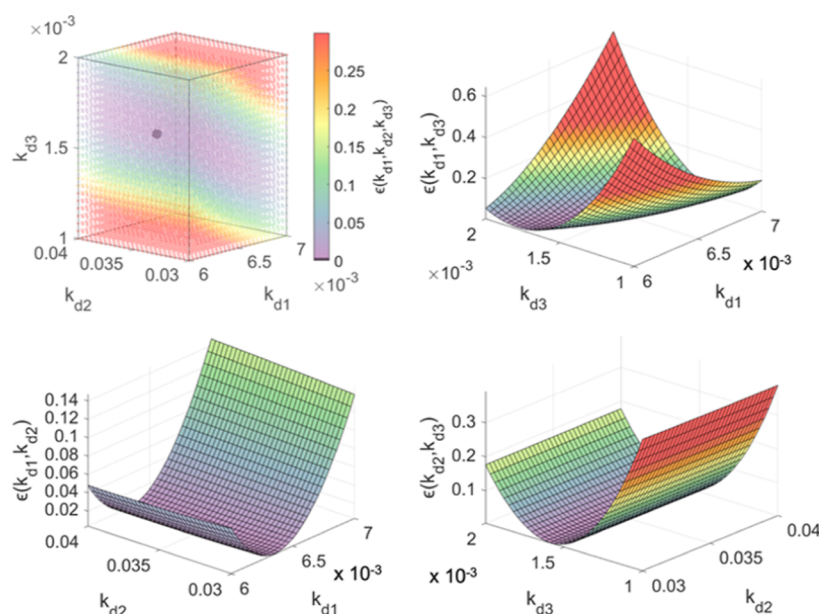
Figure 1. Minimum of the representative error function to extrapolate rate constants from convoluted kinetic data and three 3-dimensional slices of the 4-dimensional plot, where k_{d3}, k_{d2}, and k_{d1} were held constant, respectively.

Table 1. Comparison of Directly Determined and Extrapolated Mean Kinetic Rate Constants of Model System YND−BME 6a:d1-d3 in CDCl₃

method	6a:d1 avg k (s⁻¹) $t_{1/2}$ (min)	6a:d2 avg k (s⁻¹) $t_{1/2}$ (min)	6a:d3 avg k (s⁻¹) $t_{1/2}$ (min)
direct	$5.38 \pm 0.18 \times 10^{-4}$	$2.08 \pm 0.20 \times 10^{-3}$	$2.64 \pm 0.32 \times 10^{-4}$
	21.5 ± 0.7	5.6 ± 0.5	44.0 ± 5.3
extrapolated	$6.19 \pm 0.53 \times 10^{-4}$	$1.69 \pm 0.67 \times 10^{-3}$	$1.63 \pm 0.37 \times 10^{-4}$
	18.7 ± 1.5	7.6 ± 3.8	73.9 ± 17.8

Figure 2. Comparison of integrated first-order kinetics of directly measured and extrapolated retro-[4 + 2] cycloadditions of diastereomers 6a:d1-d3 in CDCl₃.

a higher stretching frequency. The same effect is observed in analogous exocyclic alkenes. Since YND−BME fragmentation was affected by delocalization/polarization of the C=C by the electron-withdrawing functional groups adjacent to the ylidene bridge (6b and 6d; Table 2), we imagined that the ring strain on the bridging ylidene would shorten the C=C bond and

effectively increase the electron density in the alkene and increase fragmentation rates. Thus, we explored a series of cyclic YND−BME substrates 6g−k (Table 3). As expected, the highly strained four- and five-membered ring substrates 6g and 6h had significantly shorter half-lives, 15.6 and 17.0 min, respectively, than the acyclic model system 6a with a half-life of 31.1 min. The extrapolated rate constants for the individual diastereomers also fit this trend. Strain was reduced in the six-membered system 6i, which provided a larger half-life than that in the model system of (44.0 min). As the bond angle of the C=C(Y) ylidene increased further with the seven- and eight-membered rings of 6j and 6k, the half-lives increased as well compared to that of the model system to 52.5 and 50.3 min, respectively. Extrapolated diastereomer rate constants showed that slower observed rates of fragmentations of the diastereomeric mixtures in 6i−k were largely due to increased populations of the slower d3 diastereomer, and the individual diastereomer rate constants were consistently slower as the ring size increased.

Ester Kinetics. Our previous report indicated that an increase in the size of the ester substituent led to a decrease in the observed rate constant for the diastereomeric mixture.[23] We postulated that this was due to larger proportions of the slower-to-fragment d3 diastereomer. We can now confirm that the extrapolated rate data for each individual diastereomer agreed with this reasoning. The individually extrapolated diastereomer rate constants remained consistent across the series 6a, 6l, and 6m, as seen in Table 4. The diastereomeric ratio of monoester substrate 6n could not be elucidated and therefore does not have comparable diastereomer data.

Table 2. Ylidene-Bridge Substituent Effects on YND−BME Fragmentation Kinetics

Y	k_{obs}^a (s⁻¹) $t_{1/2}$ (min) [d1:d2:d3:d4][b]	k_{d1} (s⁻¹) $t_{1/2\,d1}$ (min)	k_{d2} (s⁻¹) $t_{1/2\,d2}$ (min)	k_{d3} (s⁻¹) $t_{1/2\,d3}$ (min)
6a	$3.72 \pm 0.17 \times 10^{-4}$ 31.1 ± 1.4 [60:20:16:4]	$3.09 \pm 0.13 \times 10^{-4}$ 37.4 ± 1.6	$1.48 \pm 0.25 \times 10^{-3}$ 8.0 ± 1.5	$6.70 \pm 0.70 \times 10^{-5}$ 174 ± 17
6b	$1.29 \pm 0.16 \times 10^{-4}$ 89.6 ± 11 [85:9:5:1]	$1.11 \pm 0.10 \times 10^{-4}$ 98.9 ± 8.9	$5.45 \pm 6.7 \times 10^{-4}$ 24.4 ± 23.6	$4.91 \pm 0.32 \times 10^{-5}$ 235 ± 15
6c	$2.18 \pm 0.31 \times 10^{-4}$ 53.2 ± 7.3 -[c]	-	-	-
6d	$5.11 \pm 0.50 \times 10^{-5}$ 226 ± 23 [61:17:17:5]	$4.30 \pm 0.39 \times 10^{-5}$ 269 ± 25	$3.88 \pm 2.3 \times 10^{-4}$ 31.1 ± 20.8	$9.09 \pm 2.3 \times 10^{-6}$ 1280 ± 309
6e	$1.64 \pm 0.27 \times 10^{-4}$ 70.6 ± 11 [45:24:23:8]	$1.37 \pm 0.40 \times 10^{-4}$ 84.9 ± 23.9	$8.96 \pm 5.9 \times 10^{-4}$ 13.6 ± 9.8	$3.23 \pm 1.0 \times 10^{-5}$ 361 ± 113
6f	$5.83 \pm 0.70 \times 10^{-5}$ 199 ± 23 -[c]	-	-	-

[a]Our previous report[23] provided k_{obs} values from linear fits of the curved integrated rate data for the fragmentation of the mixture of diastereomers taken to 90% completion. Herein, we report more representative k_{obs} values obtained from the reaction taken to 50% completion. [b]Diastereomeric ratios determined by ¹H NMR. [c]A complex mixture of eight diastereomers with overlapping ¹H NMR resonances was observed.

Table 3. Ylidene-Bridge Ring-Strain Effects on YND−BME Fragmentation Kinetics

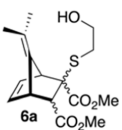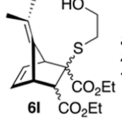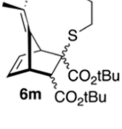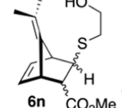| Y	k_{obs}^a (s⁻¹) $t_{1/2}$ (min) d1:d2:d3:d4 [b]	k_{d1} (s⁻¹) $t_{1/2\,d1}$ (min)	k_{d2} (s⁻¹) $t_{1/2\,d2}$ (min)	k_{d3} (s⁻¹) $t_{1/2\,d3}$ (min)
6g	$7.41 \pm 0.31 \times 10^{-4}$ 15.6 ± 0.7 66:17:13:4	$5.83 \pm 0.73 \times 10^{-4}$ 19.9 ± 2.3	$2.26 \pm 1.40 \times 10^{-3}$ 5.9 ± 4.5	$3.72 \pm 2.10 \times 10^{-4}$ 34.2 ± 18.9
6h	$6.82 \pm 0.10 \times 10^{-4}$ 17.0 ± 2.1 65:18:14:3	$6.67 \pm 0.53 \times 10^{-4}$ 17.3 ± 1.4	$1.69 \pm 1.30 \times 10^{-3}$ 7.3 ± 5.8	$1.21 \pm 0.31 \times 10^{-4}$ 96.5 ± 25.4
6a	$3.72 \pm 0.17 \times 10^{-4}$ 31.1 ± 1.4 60:20:16:4	$3.09 \pm 0.13 \times 10^{-4}$ 37.4 ± 1.6	$1.48 \pm 0.25 \times 10^{-3}$ 8.0 ± 1.5	$6.70 \pm 0.55 \times 10^{-5}$ 174 ± 17
6i	$2.63 \pm 0.24 \times 10^{-4}$ 44.0 ± 3.9 59:15:23:3 [c]	$2.60 \pm 0.47 \times 10^{-4}$ 44.5 ± 7.8	$1.16 \pm 0.34 \times 10^{-3}$ 10.1 ± 3.1	$7.03 \pm 1.10 \times 10^{-5}$ 165 ± 26
6j	$2.20 \pm 0.17 \times 10^{-4}$ 52.5 ± 4.0 45:25:20:10	$1.99 \pm 0.40 \times 10^{-4}$ 58.2 ± 12.1	$7.34 \pm 2.40 \times 10^{-4}$ 13.1 ± 5.6	$3.04 \pm 0.37 \times 10^{-5}$ 380 ± 45
6k	$2.30 \pm 0.15 \times 10^{-5}$ 50.3 ± 3.3 46:30:18:6	$1.61 \pm 0.26 \times 10^{-4}$ 72.1 ± 11.4	$9.24 \pm 3.70 \times 10^{-4}$ 12.7 ± 4.7	$1.52 \pm 0.71 \times 10^{-5}$ 777 ± 349

[a]Our previous report[23] provided k_{obs} values from linear fits of the curved integrated rate data for the fragmentation of the mixture of diastereomers taken to 90% completion. Herein, we report more representative k_{obs} values obtained from the reaction taken to 50% completion. [b]Diastereomer ratios were determined from ¹H NMR resonances of alkene protons. [c]¹H NMR resonances for the signals corresponding to **d1** and **d2** were slightly overlapping.

However, the observed rate constant was significantly (3 orders of magnitude) slower than any of the diester rate constants, and the observed half-life of the diastereomeric mixture was measured to be 11,000 min.

Diastereomer Assignment. Our preliminary report explained our diastereomer assignment of **6a:d1-4** based on two factors: (1) the precedence in the OND systems[11] and (2) the relative rate of appearance and abundance of *cis*- versus *trans*-**7** (the maleate and fumarate isomers, respectively) in the fragmentation products. No published spectra existed confirming the stereochemical configuration of the maleate/fumarate products of fragmentation. Our original assignment of the *syn* versus *anti* diastereomers was further confirmed by identifying *cis*-**7** (maleate) as the major isomer of fragmentation through NOESY correlation (Figure S3), solidifying the major diastereomer **6a:d1** as an *anti* diastereomer (see the Supporting Information for more details).

While exploring propanethiol (PT) as a steric analogue for BME as a nucleophile (vide infra), a diastereomeric mixture of YND-PT adducts (**8a**, Scheme 5) was prepared. The YND-PT system proved chromatographically separable into three fractions, eachenriched with diastereomer **8a:d1**, **d2**, and **d3**. NOESY correlations between the exo-proton alpha to the methyl ester and the methyl protons on the top of the ylidene bridge and the alpha protons of the thioether chain confirmed the structure of diastereomer **8a:d1** as the *syn*-exo diastereomer (Figure 3A). This was the predominantly formed

diastereomer (38% of the diastereomeric mixture) and the second fastest to fragment in DMSO-d_6 ($t_{1/2}$ = 34.7 min; Table 5). A NOESY correlation between the exo-proton alpha to the methyl ester and the methyl protons on the top of the ylidene bridge and a correlation between the alpha protons of the thioether chain and the olefin proton identified the structure of diastereomer **8a:d2** as the *anti*-endo diastereomer and was the fastest to fragment in DMSO-d_6 ($t_{1/2}$ = 5 min; Table 5) (Figure 3B). Finally, a NOESY correlation between the endo-proton alpha to the methyl ester and the olefin proton confirmed the structure of diastereomer **8a:d3** as *anti*-exo (Figure 3C) and was the slowest to fragment ($t_{1/2}$ = 139 min; Table 5) (see the Supporting Information for full analysis of NOESY spectra).

Computational Investigation. To further investigate the fragmentation kinetics of the model YND system **6a**, the free energy of activation of a retro-[4 + 2] cycloaddition reaction was calculated for each diastereomer **6a:d1-4**. Our initial report provided assignments for the **6a:d2** and **6a:d3** diastereomers that were incorrect. The assignment of the YND-PT **8a** diastereomers was used to correct the assignment of the YND−BME **6a** system, exchanging the initial structures of **6a:d2** and **6a:d3**. However, before this correction, we

**Table 4. Effect of Ester Substitution on Fragmentation Kinetics of YND−BMEs**

	k_{obs}^{a} (s⁻¹) $t_{1/2}$ (min) d1:d2:d3:d4 ^{b}	k_{d1} (s⁻¹) $t_{1/2\ d1}$ (min)	k_{d2} (s⁻¹) $t_{1/2\ d2}$ (min)	k_{d3} (s⁻¹) $t_{1/2\ d3}$ (min)
6a	$3.72 \pm 0.17 \times 10^{-4}$ 31.1 ± 1.4 $60{:}20{:}16{:}4$	$3.09 \pm 0.13 \times 10^{-4}$ 37.4 ± 1.6	$1.48 \pm 0.25 \times 10^{-3}$ 8.0 ± 1.5	$6.70 \pm 0.70 \times 10^{-5}$ 173.5 ± 18.1
6l	$3.92 \pm \times 0.79 \times 10^{-4}$ 29.6 ± 5.7 $49{:}24{:}21{:}3$	$3.16 \pm 0.47 \times 10^{-4}$ 36.6 ± 5.3	$2.11 \pm 3.23 \times 10^{-3}$ 6.75 ± 7.82	$6.61 \pm 1.41 \times 10^{-5}$ 175.6 ± 39.1
6m	$2.56 \pm 0.66 \times 10^{-4}$ 45.4 ± 12.0 $43{:}23{:}27{:}7$	$2.98 \pm 0.39 \times 10^{-4}$ 38.9 ± 5.3	$6.60 \pm 5.55 \times 10^{-4}$ 19.3 ± 19.8	$5.22 \pm 0.70 \times 10^{-5}$ 222.7 ± 28.9
6n	$1.05 \pm 0.29 \times 10^{-6}$ 11000 ± 2800 unknown ^{c}	--		--

^{a}Our previous report[23] provided k_{obs} values from linear fits of the curved integrated rate data for the fragmentation of the mixture of diastereomers taken to 90% completion. Herein, we report more representative k_{obs} values obtained from the reaction taken to 50% completion. ^{b}Diastereomer ratios were determined from ^{1}H NMR resonances of alkene protons. ^{c}Diastereomer ratios of **6n** were unable to be determined from the ^{1}H NMR spectrum.

explored four alternate mechanisms, trying to find a lower energy transition state to explain the large discrepancy in the experimental and computational free energies of activation for the *anti*-exo diastereomer. This exploration of the potential energy surface (PES) can be found in the Supporting Information. DFT calculations were performed using GAMESS 2020 R1.[28] Geometries were first optimized using the density functional ωB97X-D[29] and the 6-31+G(d) basis set, and the solvation effects were corrected for using DMSO implicit solvation[30] and the 6-311+G(d,p) basis set. Conformational searches were performed using CREST,[31] and the generated conformers were re-ranked using single-point calculations with ωB97X-D/6-311+G(d,p) and DMSO implicit solvent. Later, for comparison, geometries were also optimized using the density functionals, M06-2X[32] and B3LYP,[33,34] and the 6-31+G(d) basis set. Solvation effects were again corrected for using DMSO implicit solvation and the 6-311+G(d,p) basis set. Free energies were also further corrected by single-point calculations using domain-based local pair natural orbital coupled cluster method DLPNO-CCSD(T)[35,36] and the def2-TZVPP basis set performed by ORCA v5.0[37,38] based on geometries optimized by all three functionals (see the Supporting Information for more details).

For the model YND system **6a**, using the DFT functional ωB97X-D, the free energy of activation for the retro-[4 + 2]

Scheme 5. Preparation and Fragmentation of YND-PT Diastereomers 8a:d1-4
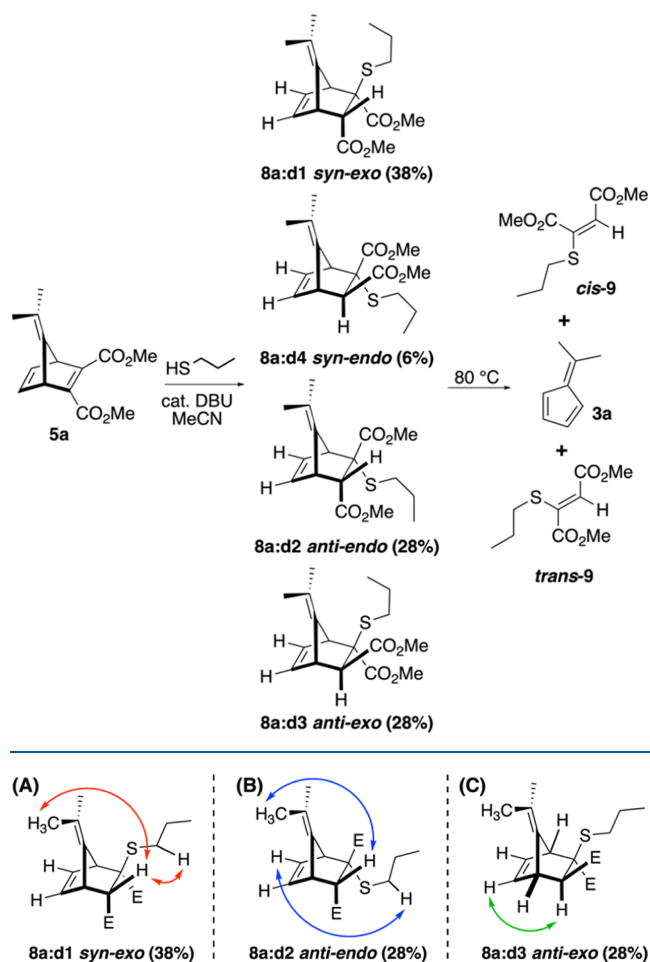
Figure 3. Observed NOESY correlations elucidating the structures of diastereomers **8a:d1-d3** [E = CO$_2$Me].

cycloaddition in kcal/mol for **6a:d1** is 27.8, **6a:d2** is 27.7, **6a:d3** is 30.5, and **6a:d4** is 30.3 (Figure 4). Examining these computational free energies of activation, the values for **6a:d1** and **6a:d2** are nearly identical, as are **6a:d3** and **6a:d4**. This suggests that the density functional ωB97X-D is correctly differentiating the two diastereomers that are faster to fragment from the two diastereomers that are slower to fragment but cannot adequately distinguish them further. Furthermore, using the density functional ωB97X-D provides a relatively accurate estimate for the experimental free energy of activation of diastereomers **6a:d1**, **6a:d2**, and **6a:d3** individually as the energies are within 1.0, 2.4, and 2.6 kcal/mol, respectively. We next utilized the density functionals M06-2X and B3LYP for comparison (Table 6). The density functional B3LYP only identified the two faster fragmenting diastereomers and the two slower fragmenting diastereomers, but the calculated free energies of activation for each diastereomer were more than 10 kcal/mol lower than the experimental values. The density functional M06-2X was overall more accurate when comparing **6a:d1**, **6a:d2**, and **6a:d3** individually with the experimental free energies of activation as the energies were within 1.9, 1.2, and 0.1 kcal/mol, respectively. However, the DFT functional M06-2X identified **6a:d1** and **6a:d2** as faster to fragment than the other two diastereomers (**6a:d3** and **6a:d4**) but calculated

Table 5. Extrapolated and Isolated Kinetic Rate Constants of YND-PT Diastereomers 8a:d1−d3 in DMSO-d_6

system (solvent) method	d1 k_{d1} (s^{-1}) $t_{1/2}$ (min)	d2 k_{d2} (s^{-1}) $t_{1/2}$ (min)	d3 k_{d3} (s^{-1}) $t_{1/2}$ (min)
8a (DMSO-d_6) extrapolated	$3.28 \pm 0.25 \times 10^{-4}$ 35.3 ± 2.5	$1.66 \pm 0.23 \times 10^{-3}$ 7.0 ± 1.0	$6.83 \pm 0.68 \times 10^{-5}$ 170 ± 17
8a (DMSO-d_6) isolated	$3.33 \pm 0.25 \times 10^{-4}$ 34.7 ± 2.6	$2.33 \pm 0.15 \times 10^{-3}$ 5.0 ± 0.3	$8.33 \pm 1.02 \times 10^{-5}$ 139 ± 17
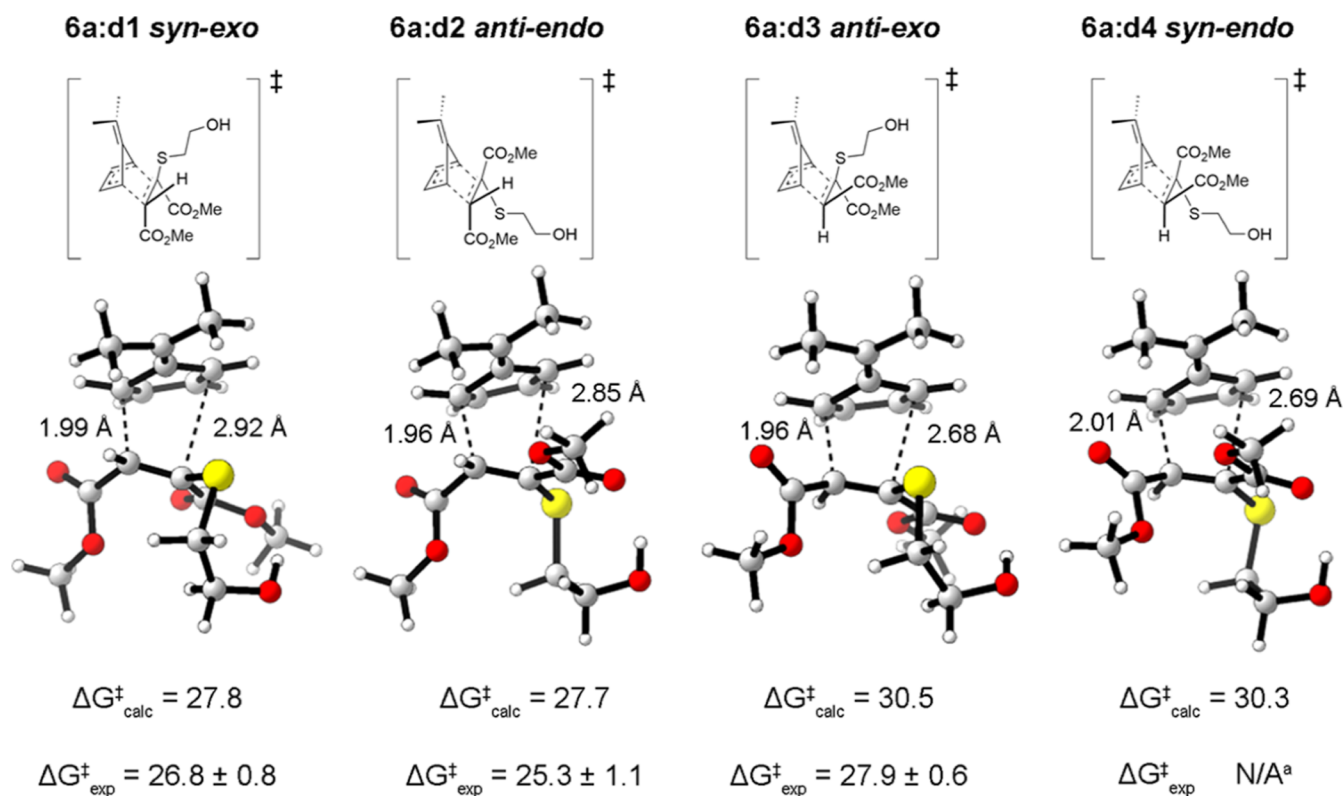
Figure 4. Corrected assignment of diastereomers with calculated and experimental free energies of activation (ωB97X-D). Energies in kcal/mol. Energies were calculated at 25 °C and 1 atm with DMSO implicit solvent, and the experimental energies were calculated at 25 °C using the parameters from Arrhenius plot.[23] [a]experimental free energy of activation for **6a:d4** was not measured because this diastereomer was rerecovered as only 4% of the total diastereomeric mixture, and it fragmented much slower relative to the other three diastereomers.

Table 6. Comparison of DFT Functionals for Computed 6a:d1-4 TS Energies[a]

diast.	experimental $\Delta G^{\ddagger}$	B3LYP $\Delta G^{\ddagger}$	nascent bond lengths (Å)	DLPNO-CCSD(T) corrected $\Delta G^{\ddagger}$	M06-2X $\Delta G^{\ddagger}$	nascent bond lengths (Å)	DLPNO-CCSD(T) corrected $\Delta G^{\ddagger}$	ωB97X-D $\Delta G^{\ddagger}$	nascent bond lengths (Å)	DLPNO-CCSD(T) corrected $\Delta G^{\ddagger}$
6a:d1	26.8	15.2	1.95/3.09	29.4	24.9	1.94/2.78	28.1	27.8	1.99/2.92	28.6
6a:d2	25.3	15.7	1.90/3.05	31.6	26.5	1.92/2.73	29.7	27.7	1.96/2.85	30.1
6a:d3	27.9	18.5	1.88/2.84	34.3	28.0	2.03/2.28	30.0	30.5	1.96/2.68	32.6
6a:d4	—[b]	17.5	1.92/2.86	31.3	27.2	2.02/2.53	29.9	30.3	2.01/2.69	30.9

[a]Structures and vibrational frequencies were optimized with the 6-31+G(d) basis set, and electronic energies were calculated with the 6-311+G(d,p) basis set and DMSO implicit solvent. $\Delta G^{\ddagger}$ values are given in kcal/mol. [b]The experimental free energy of activation for **6a:d4** was not measured because this diastereomer was rerecovered as only 4% of the total diastereomeric mixture, and it fragmented much slower relative to the other three diastereomers.

the free energy of activation for the fragmentation of **6a:d1** to be to be 1.6 kcal/mol lower than that of **6a:d2**, which is the opposite of what is observed experimentally. Likewise, with the M06-2X functional, **6a:d4** is calculated to be faster to fragment than **6a:d3**, contrary to the experimental data. Finally, we looked at correcting the structures optimized by each DFT

functional with single-point calculations using a DLPNO-CCSD(T)) and the basis set def2-TZVPP. Corrections on the B3LYP-optimized values greatly helped improve the similarity between the experimental and calculated free energies of activation for all four diastereomers, with all the computational values being within a difference of 1.2−5 kcal/mol of the

Table 7. Comparison of Kinetic Rate Constants of YND−BME 6a:d1-d3 and YND-PT 8a:d1-d3 in CDCl$_3$ and DMSO-d_6

system (solvent) method	diastereomer		
	k_{d1} (s^{-1})	k_{d2} (s^{-1})	k_{d3} (s^{-1})
6a (DMSO-d_6) extrapolated[a]	$3.09 \pm 0.13 \times 10^{-4}$	$1.48 \pm 0.25 \times 10^{-3}$	$6.70 \pm 0.65 \times 10^{-5}$
8a (DMSO-d_6) isolated[b]	$3.33 \pm 0.25 \times 10^{-4}$	$2.33 \pm 0.15 \times 10^{-3}$	$8.33 \pm 1.02 \times 10^{-5}$
6a (CDCl$_3$) direct[c]	$5.38 \pm 0.18 \times 10^{-4}$	$2.08 \pm 0.20 \times 10^{-3}$	$2.64 \pm 0.32 \times 10^{-4}$
8a (CDCl$_3$) isolated[b]	$2.75 \pm 0.14 \times 10^{-4}$	$2.30 \pm 0.07 \times 10^{-3}$	$8.47 \pm 0.46 \times 10^{-5}$

[a]Rate constants are extrapolated from combined convoluted rate data of a mixture of diastereomers **d1**−**d3** using kinetic simulations. [b]Rate constants are derived from kinetics measured of isolated diastereomer-enriched samples. [c]Rate constants are derived from kinetics measured from the direct measurement of single resolvable diastereomer ^{1}H NMR resonances in a mixture of diastereomers **d1**−**d3**.

experimental values. However, none of the corrected values matched the relative ranking of the experimental free energies of activation for fragmentation across the four diastereomers. Regardless of which DFT functional optimized the structures of diastereomers, the DLPNO-CCSD(T)/def2-TZVPP-corrected energies mis-ranked the free energies of activation for the fragmentation of the two faster and two slower diastereomers (Table 6). Therefore, out of the three density functionals examined and DLPNO-CCSD(T) corrections, the uncorrected ωB97X-D best describes the activation barriers of fragmentation for **6a:d1**−**d4** relative to one another, but the functional is still unable to identify the stereoelectronic effects leading to a difference between the two fast diastereomers (**6a:d2** and **6a:d1**) and between the two slower diastereomers (**6a:d3** and **6a:d4**). We are continuing to study this system both experimentally and computationally in an effort to discern the factors leading to the difference in diastereomer rates of fragmentation.

Solvent Effects and Hydrogen-Bonding. In the course of exploring the model system **6a**, the rate constants were experimentally measured to be higher with chloroform-d as the solvent versus DMSO-d_6 for all three diastereomers (Table 7). This contradicts the hypothesis that a more polar solvent would stabilize the buildup of charge in the computed asynchronous transition state structures of a retro-[4 + 2] cycloaddition reaction.[39] While the degree of asynchronicity was observed to vary depending on the DFT functional chosen as seen in the ratio of nascent bond lengths (Table 5), with the B3LYP functional computing the most asynchronous transition state structures for all diastereomers, all functionals did provide asynchronous transition state structures. The major diastereomer for the model system was examined with respect to Mulliken charges,[40] using the ωB97X-D functional, in the reactant (**6a:d1**) and the transition state structure **TS1**. As seen in Figure 5, the fulvene portion has an increase in positive charge of 0.40 e on going from YND−BME **6a:d1** to the transition state structure **TS1**. These computational results suggest that in the transition state structure, there is an increase in positive charge on the fulvene portion of the structure and thus, an equal increase of negative charge in the forming alkene portion of the structure.

We postulated that an intramolecular hydrogen bond between the pendant alcohol of the added BME and the proximal ester was able to stabilize the buildup of negative charge on the carbonyl oxygen, thus lowering the activation energy. Evidently, this hydrogen-bond stabilization was only occurring in CDCl$_3$ (Figure 6A). In DMSO, this pendant alcohol would be solvated (Figure 6B). To test this hypothesis, we experimentally studied the YND-PT system **8a** (Figure 6C) as a steric analogue of the YND−BME system, which could not exhibit this hydrogen-bond stabilization.
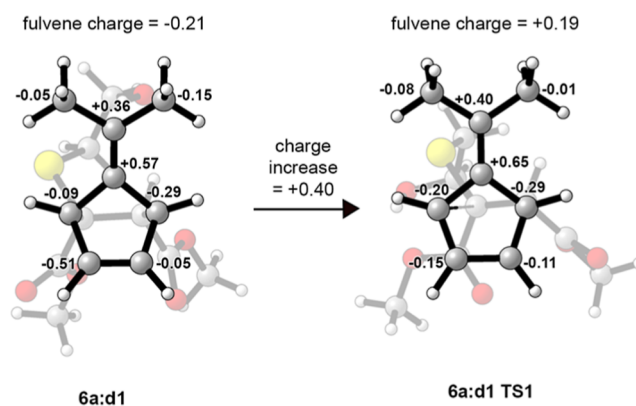

Figure 5. Charge distribution in **6a:d1** and **TS1-6a:d1**. Charges in electrons and hydrogens summed into carbons.
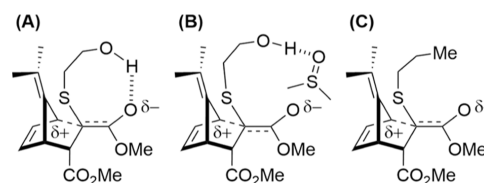

Figure 6. Transition state charge buildup of YND−BME **6a** in (A) CDCl$_3$, (B) DMSO-d_6, and (C) YND-PT **8a** (only the **d1** diastereomer is shown for clarity).

Model YND **5a** was reacted with PT as a nucleophile with the DBU catalyst in acetonitrile and resulted in a diastereomeric mixture of YND-PT **8a:d1-4**. As mentioned previously, it was possible to chromatographically isolate the individual fractions enriched with diastereomers **8a:d1**, **d2**, and **d3**. The mixture of diastereomers and the isolated samples of diastereomers were each subjected to kinetic fragmentation and extrapolation experiments in DMSO-d_6 (Scheme 5).

The results of extrapolated rate constants derived from our kinetic simulation method aligned very well with the isolated diastereomer rate constants. As shown in Table 5, the extrapolated values for the rate constant k_{d1} are within 3% of the isolated individual diastereomer rate constant, k_{d3} is within 12%, and the rate constant k_{d2} is within 30% of the isolated individual diastereomer rate constant. These results further substantiate our kinetic simulations as a viable tool for extrapolating rate constants from convoluted observed kinetic data.

The YND-PT system **8a** was also fragmented and analyzed in CDCl$_3$. YND-PT **8a** fulfilled the expectation that the more polar DMSO solvent would result in an increase in the rate of fragmentation only in **8a:d1** with the rate constant modestly increasing from 2.75×10^{-4} to 3.33×10^{-4} s^{-1} (Table 7).

Furthermore, the respective rate constants, of each diastereomer of **6a** and **8a** in DMSO were observed to be roughly equivalent, for example, **6a:d1**; $k = 3.09 \times 10^{-4}$ and **8a:d1**; $k = 3.33 \times 10^{-4}$ (Table 7), suggesting that in DMSO, the pendant alcohol is not undergoing hydrogen bonding with the carbonyl oxygen, rendering the two systems effectively equivalent with regard to the stabilization of charge by the pendant alcohol.

Hammett Study. Finally, a Hammett study was performed to gain further insight into the substituent effects on the rate of YND−BME adduct fragmentation. The added asymmetry created by the four substituted phenyl rings on the ylidene created complex mixtures of eight diastereomers. However, in substrates **6o−6u**, proton integration ratios showed consistent diastereomer ratios across the substrate scope (Figure S16). Since the rate of fragmentation has proven to vary greatly for the different diastereomers, the consistency in diastereomer ratios allowed for a reasonable comparison of the observed rate of the mixture. As seen in Table 8, the para-substitution of

Table 8. Hammett Substrate Kinetics Data

Figure 7. Hammett plot versus sigma parameter.

^{a}The temperature was increased to 90 °C for the Hammett study substrates such that the study of slower-to-fragment substrates could be completed in overnight NMR experiments. ^{b}Our previous report[23] provided k_{obs} values from linear fits of the curved integrated rate data for the fragmentation of the mixture of diastereomers taken to 90% completion. Herein, we report more representative k_{obs} values obtained from the reaction taken to 50% completion.

electron-donating groups accelerated the fragmentation with the fastest rate observed for dimethylamino-substituted **6o** ($t_{1/2}$ = 5.9 min), while the slowest rate of fragmentation was observed for the CF$_3$-substituted substrate **6u** ($t_{1/2}$ = 70 min). These results further support the theoretical result showing an increase of positive charge (0.40e) in the fulvene portion of the structures on going from YND−BME to the transition state (Figure 5). The larger ρ value of −0.78 derived from the Hammett plot[41] (Figure 7) in comparison to the OND system (ρ = −0.49)[14] further supports an asynchronous transition state structure. Furthermore, the larger ρ value is in alignment with the fact that the change in charge on the analogous furan portion of the OND system also showed an increase of 0.20e versus 0.40e for the fulvene portion of the YND.[14] Finally, in the OND system, theoretical calculations for the retro-[4 + 2] transition state structure gave nascent bond lengths of 1.91 and 2.53 Å in the model system,[12] while all the diastereomers of the model YND system (**6a**) have more developed transition state structures (Table 5 and Figure 5), with the most
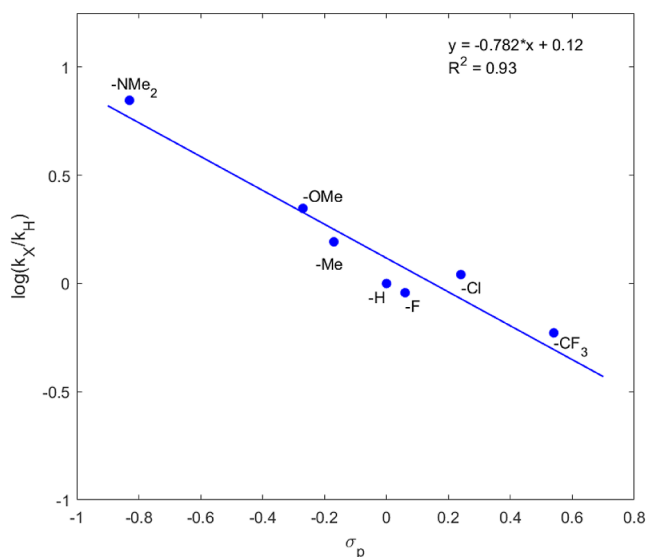
asynchronous (**6a:d2**) having nascent bond lengths of 1.96 and 2.85 Å (ωB97X-D functional).

■ CONCLUSIONS

Thiol nucleophiles BME and propane thiol added to symmetric YND substrates yield a mixture of four diastereomers and added to asymmetric YNDs yield up to eight diastereomers of YND-thiol adducts. These YND thiol adduct diastereomers were observed to fragment via retro-[4 + 2] reactions at rates which can differ by nearly 2 orders of magnitude between the fastest and slowest diastereomers. Kinetic simulations were conducted to extrapolate rate constants and were determined to match individually measured values, thereby validating our methodology. Computational DFT explorations and a Hammett study support the view that the fragmentation reaction proceeds through an asynchronous retro-[4 + 2] transition state, with a buildup of positive charge in the fulvene portion of the molecule. The structures and functional groups which increase the charge density in the ylidene atop the YND bridge stabilize this positive charge buildup and accelerate the fragmentation reaction. Electron-withdrawing functionalities decelerate the fragmentation. This work has helped gain insight into how YNDs could be used as tunable click and clip linkages for a variety of applications.

■ ASSOCIATED CONTENT

Data Availability Statement

The data underlying this study are available in the published article and its Supporting Information.

Ⓢ Supporting Information

The Supporting Information is available free of charge at https://pubs.acs.org/doi/10.1021/acs.joc.3c00980.

Full experimental details, including synthetic and kinetic procedures and characterization details (PDF)

Full computational methods, energies, and Cartesian coordinates for all optimized structures and transition state structures and ^{1}H and ^{13}C NMR spectra for new compounds (PDF)

AUTHOR INFORMATION

Corresponding Author

Daniel A. Bercovici − *Department of Chemistry and Biochemistry, California Polytechnic State University, San Luis Obispo, California 93407, United States;* orcid.org/0000-0002-8502-9560; Email: dbercovi@calpoly.edu

Authors

Abigail D. Richardson − *Department of Chemistry and Biochemistry, California Polytechnic State University, San Luis Obispo, California 93407, United States;* Present Address: The University of Manchester, Manchester M13 9PL, United Kingdom; orcid.org/0000-0001-5900-5357

Scott J. L'Heureux − *Department of Chemistry and Biochemistry, California Polytechnic State University, San Luis Obispo, California 93407, United States;* orcid.org/0000-0002-2299-2253

Ava M. Henry − *Department of Chemistry and Biochemistry, California Polytechnic State University, San Luis Obispo, California 93407, United States;* Present Address: University of California, San Diego, La Jolla, CA 92093, United States.

Elizabeth A. McDonough − *Department of Chemistry and Biochemistry, California Polytechnic State University, San Luis Obispo, California 93407, United States;* Present Address: Polycoat Products, Santa Fe Springs, CA 90670, United States.

Cameron J. Fleischer − *Department of Chemistry and Biochemistry, California Polytechnic State University, San Luis Obispo, California 93407, United States*

Cameron C. McMullen − *Department of Chemistry and Biochemistry, California Polytechnic State University, San Luis Obispo, California 93407, United States*

Trevor R. Reynafarje − *Department of Chemistry and Biochemistry, California Polytechnic State University, San Luis Obispo, California 93407, United States*

Gisele P. Guerrero − *Department of Chemistry and Biochemistry, California Polytechnic State University, San Luis Obispo, California 93407, United States*

Quinn E. Williams − *Department of Chemistry and Biochemistry, California Polytechnic State University, San Luis Obispo, California 93407, United States*

Qingyang Zhou − *Department of Chemistry and Biochemistry, University of California, Los Angeles, Los Angeles, California 90095, United States*

David M. Malouf − *Department of Chemistry and Biochemistry, California Polytechnic State University, San Luis Obispo, California 93407, United States;* Present Address: Marshall B. Ketchum Southern California College of Optometry, Fullerton, CA 92831, United States.

Spencer E. Thurman − *Department of Chemistry and Biochemistry, California Polytechnic State University, San Luis Obispo, California 93407, United States*

Julia E. Soeller − *Department of Chemistry and Biochemistry, California Polytechnic State University, San Luis Obispo, California 93407, United States*

Jerry Y. Sheng − *Department of Chemistry and Biochemistry, California Polytechnic State University, San Luis Obispo, California 93407, United States;* Present Address: San Francisco State University, San Francisco, CA 94132, United States.

Erica A. Medhurst − *Department of Chemistry and Biochemistry, California Polytechnic State University, San Luis Obispo, California 93407, United States*

Angel E. Canales − *Department of Chemistry and Biochemistry, California Polytechnic State University, San Luis Obispo, California 93407, United States;* Present Address: Brightseed Inc., South San Francisco, CA, 94080, United States.

Ty B. Cecil − *Department of Chemistry and Biochemistry, California Polytechnic State University, San Luis Obispo, California 93407, United States*

K. N. Houk − *Department of Chemistry and Biochemistry, University of California, Los Angeles, Los Angeles, California 90095, United States*

Philip J. Costanzo − *Department of Chemistry and Biochemistry, California Polytechnic State University, San Luis Obispo, California 93407, United States*

Complete contact information is available at:
https://pubs.acs.org/10.1021/acs.joc.3c00980

Notes

The authors declare no competing financial interest.

REFERENCES

(1) Kolb, H. C.; Finn, M. G.; Sharpless, K. B. Click Chemistry:Diverse Chemical Function Froma Few Good Reactions. *Angew. Chem., Int. Ed.* **2001**, *40*, 2004−2021.

(2) NobelPrize.org. *Nobel Prize Outreach AB 2022*, 2022.

(3) Shieh, P.; Hill, M. R.; Zhang, W.; Kristufek, S. L.; Johnson, J. A. Clip Chemistry: Diverse (Bio)(Macro)Molecular and Material Function through Breaking Covalent Bonds. *Chem. Rev.* **2021**, *121*, 7059−7121.

(4) Kumler, M. S.; Skinner, N. M.; Meyersohn, M. S.; Colt, T. A.; Valverde, M.; Powell, C. E.; Costanzo, P. J. Trials and Adventures of the Synthesis and Evaluation of Amphiphilic Graft Copolymers with Dynamic Topology. *J. Polym. Sci.* **2022**, *60*, 3117−3127.

(5) Bisbjerg, G.; Brown, G. W.; Pham, K. S.; Kock, R. A.; Ramos, W.; Patierno, J. A.; Bautista, A.; Zawalick, N. M.; Vigil, V.; Padrnos, J. D.; Mathers, R. T.; Heying, M. D.; Costanzo, P. J. Exploring Polymer Solubility with Thermally-Responsive Diels-Alder Monomers: Revisiting the Monkey's Fist. *J. Polym. Sci.* **2022**, *60*, 175−187.

(6) Wilborn, E. G.; Gregory, C. M.; Machado, C. A.; Page, T. M.; Ramos, W.; Hunter, M. A.; Smith, K. M.; Gosting, S. E.; Tran, R.; Varney, K. L.; Savin, D. A.; Costanzo, P. J. Unraveling Polymer Structures with RAFT Polymerization and Diels-Alder Chemistry. *Macromolecules* **2019**, *52*, 1308−1316.

(7) Amato, D. N.; Strange, G. A.; Swanson, J. P.; Chavez, A. D.; Roy, S. E.; Varney, K. L.; Machado, C. A.; Amato, D. V.; Costanzo, P. J. Synthesis and Evaluation of Thermally-Responsive Coatings Based upon Diels-Alder Chemistry and Renewable Materials. *Polym. Chem.* **2014**, *5*, 69−76.

(8) Swanson, J. P.; Rozvadovsky, S.; Seppala, J. E.; Mackay, M. E.; Jensen, R. E.; Costanzo, P. J. Development of Polymeric Phase

Change Materials on the Basis of Diels-Alder Chemistry. *Macromolecules* **2010**, *43*, 6135−6141.

(9) Dirlam, P. T.; Strange, G. A.; Orlicki, J. A.; Wetzel, E. D.; Costanzo, P. J. Controlling Surface Energy and Wetability with Diels-Alder Chemistry. *Langmuir* **2010**, *26*, 3942−3948.

(10) Hong, V.; Kislukhin, A. A.; Finn, M. G. Thiol-Selective Fluorogenic Probes for Labeling and Release. *J. Am. Chem. Soc.* **2009**, *131*, 9986−9994.

(11) Kislukhin, A. A.; Higginson, C. J.; Hong, V. P.; Finn, M. G. Degradable Conjugates from Oxanorbornadiene Reagents. *J. Am. Chem. Soc.* **2012**, *134*, 6491−6497.

(12) Fell, J. S.; Lopez, S. A.; Higginson, C. J.; Finn, M. G.; Houk, K. N. Theoretical Analysis of the Retro-Diels−Alder Reactivity of Oxanorbornadiene Thiol and Amine Adducts. *Org. Lett.* **2017**, *19*, 4504−4507.

(13) Aioub, A. G.; Higginson, C. J.; Finn, M. G. Traceless Release of Alcohols Using Thiol-Sensitive Oxanorbornadiene Linkers. *Org. Lett.* **2018**, *20*, 3233−3236.

(14) De Pascalis, L.; Yau, M. K.; Svatunek, D.; Tan, Z.; Tekkam, S.; Houk, K. N.; Finn, M. G. The Influence of Substitution on Thiol-Induced Oxanorbornadiene Fragmentation. *Org. Lett.* **2021**, *23*, 3751−3754.

(15) Fiedler, J. D.; Higginson, C.; Hovlid, M. L.; Kislukhin, A. A.; Castillejos, A.; Manzenrieder, F.; Campbell, M. G.; Voss, N. R.; Potter, C. S.; Carragher, B.; Finn, M. G. Engineered Mutations Change the Structure and Stability of a Virus-like Particle. *Biomacromolecules* **2012**, *13*, 2339−2348.

(16) Higginson, C. J.; Eno, M. R.; Khan, S.; Cameron, M. D.; Finn, M. G. Albumin-Oxanorbornadiene Conjugates Formed Ex Vivo for the Extended Circulation of Hydrophilic Cargo. *ACS Chem. Biol.* **2016**, *11*, 2320−2327.

(17) Sanhueza, C. A.; Baksh, M. M.; Thuma, B.; Roy, M. D.; Dutta, S.; Préville, C.; Chrunyk, B. A.; Beaumont, K.; Dullea, R.; Ammirati, M.; Liu, S.; Gebhard, D.; Finley, J. E.; Salatto, C. T.; King-Ahmad, A.; Stock, I.; Atkinson, K.; Reidich, B.; Lin, W.; Kumar, R.; Tu, M.; Menhaji-Klotz, E.; Price, D. A.; Liras, S.; Finn, M. G.; Mascitti, V. Efficient Liver Targeting by Polyvalent Display of a Compact Ligand for the Asialoglycoprotein Receptor. *J. Am. Chem. Soc.* **2017**, *139*, 3528−3536.

(18) Schudel, A.; Chapman, A. P.; Yau, M. K.; Higginson, C. J.; Francis, D. M.; Manspeaker, M. P.; Avecilla, A. R. C.; Rohner, N. A.; Finn, M. G.; Thomas, S. N. Programmable Multistage Drug Delivery to Lymph Nodes. *Nat. Nanotechnol.* **2020**, *15*, 491−499.

(19) Higginson, C. J.; Kim, S. Y.; Peláez-Fernández, M.; Fernández-Nieves, A.; Finn, M. Modular Degradable Hydrogels Based on Thiol-Reactive Oxanorbornadiene Linkers. *J. Am. Chem. Soc.* **2015**, *137*, 4984−4987.

(20) Johnson, M. D.; Lloyd, J.; Tekkam, S.; Crooke, S. N.; Witherden, D. A.; Havran, W. L.; Finn, M. G. Degradable Hydrogels for the Delivery of Immune-Modulatory Proteins in the Wound Environment. *ACS Appl. Bio Mater.* **2020**, *3*, 4779−4788.

(21) Soret, A.; Müller, C.; Guillot, R.; Blanco, L.; Deloisy, S. Short and Efficient Synthesis of 2H-Pyrroles from 7-Oxanorbornadiene Derivatives. *Tetrahedron* **2011**, *67*, 698−705.

(22) Tekkam, S.; Finn, M. G. Synthesis and Reactivity of 5 - Substituted Furfuryl Carbamates via Oxanorbornadienes. *Org. Lett.* **2017**, *19*, 2833−2836.

(23) Malouf, D. M.; Richardson, A. D.; L'Heureux, S. J.; McDonough, E. A.; Henry, A. M.; Sheng, J. Y.; Medhurst, E. A.; Canales, A. E.; Fleischer, C. J.; Cecil, T. B.; Thurman, S. E.; McMullen, C. C.; Costanzo, P. J.; Bercovici, D. A. Ylidenenorbornadiene Carboxylates: Experimental Kinetic Analysis of a Nucleophile-Induced Fragmentation Reaction. *Org. Lett.* **2022**, *24*, 2793−2797.

(24) Gugelchuk, M. M.; Chan, P. C. M.; Sprules, T. J. Can Remote Substituent Effects Influence Reactivity and Stereoselectivity in the Diels-Alder Cycloadditions of p-Substituted 6-Phenyl-6-Methylfulvenes? *J. Org. Chem.* **1994**, *59*, 7723−7731.

(25) Von Arx, K. B.; Manock, J. J.; Huffman, S. W.; Messina, M. Using Limited Concentration Data for the Determination of Rate Constants with the Genetic Algorithm. *Environ. Sci. Technol.* **1998**, *32*, 3207−3212.

(26) Bellamy, L. J. *The Infrared Spectra of Complex Molecules*, 3rd ed.; Chapman & Hall: London, 1975.

(27) Colthup, N. B.; Daly, L. H. *Introduction to Infrared and Raman Spectroscopy*, 3rd ed.; Academic Press: San Diego, 1990.

(28) Barca, G. M. J.; Bertoni, C.; Carrington, L.; Datta, D.; De Silva, N.; Deustua, J. E.; Fedorov, D. G.; Gour, J. R.; Gunina, A. O.; Guidez, E.; Harville, T.; Irle, S.; Ivanic, J.; Kowalski, K.; Leang, S. S.; Li, H.; Li, W.; Lutz, J. J.; Magoulas, I.; Mato, J.; Mironov, V.; Nakata, H.; Pham, B. Q.; Piecuch, P.; Poole, D.; Pruitt, S. R.; Rendell, A. P.; Roskop, L. B.; Ruedenberg, K.; Sattasathuchana, T.; Schmidt, M. W.; Shen, J.; Slipchenko, L.; Sosonkina, M.; Sundriyal, V.; Tiwari, A.; Galvez Vallejo, J. L.; Westheimer, B.; Włoch, M.; Xu, P.; Zahariev, F.; Gordon, M. S. Recent Developments in the General Atomic and Molecular Electronic Structure System. *J. Chem. Phys.* **2020**, *152*, 154102.

(29) Chai, J. Da; Head-Gordon, M. Long-Range Corrected Hybrid Density Functionals with Damped Atom-Atom Dispersion Corrections. *Phys. Chem. Chem. Phys.* **2008**, *10*, 6615−6620.

(30) Cancès, E.; Mennucci, B.; Tomasi, J. A New Integral Equation Formalism for the Polarizable Continuum Model: Theoretical Background and Applications to Isotropic and Anisotropic Dielectrics. *J. Chem. Phys.* **1997**, *107*, 3032−3041.

(31) Pracht, P.; Bohle, F.; Grimme, S. Automated Exploration of the Low-Energy Chemical Space with Fast Quantum Chemical Methods. *Phys. Chem. Chem. Phys.* **2020**, *22*, 7169−7192.

(32) Zhao, Y.; Truhlar, D. G. The M06 suite of density functionals for main group thermochemistry, thermochemical kinetics, non-covalent interactions, excited states, and transition elements: two new functionals and systematic testing of four M06-class functionals and 12 other functionals. *Theor. Chem. Acc.* **2008**, *120*, 215−241.

(33) Lee, C.; Yang, W.; Parr, R. G. Development of the Colle-Salvetti Correlation-Energy Formula into a Functional of the Electron Density. *Phys. Rev. B* **1988**, *37*, 785−789.

(34) Becke, A. D. Density-Functional Thermochemistry. III. The Role of Exact Exchange. *J. Chem. Phys.* **1993**, *98*, 5648−5652.

(35) Liakos, D. G.; Guo, Y.; Neese, F. Comprehensive Benchmark Results for the Domain Based Local Pair Natural Orbital Coupled Cluster Method (DLPNO-CCSD(T)) for Closed- And Open-Shell Systems. *J. Phys. Chem. A* **2020**, *124*, 90−100.

(36) Riplinger, C.; Neese, F. An Efficient and near Linear Scaling Pair Natural Orbital Based Local Coupled Cluster Method. *J. Chem. Phys.* **2013**, *138*, 034106.

(37) Neese, F. The ORCA Program System. *Wiley Interdiscip. Rev.: Comput. Mol. Sci.* **2012**, *2*, 73−78.

(38) Neese, F. Software Update: The ORCA Program System— Version 5.0. *Wiley Interdiscip. Rev.: Comput. Mol. Sci.* **2022**, *12*, No. e1606.

(39) Zou, Y.; Yang, S.; Sanders, J. N.; Li, W.; Yu, P.; Wang, H.; Tang, Z.; Liu, W.; Houk, K. N. Computational Investigation of the Mechanism of Diels-Alderase PyrI4. *J. Am. Chem. Soc.* **2020**, *142*, 20232−20239.

(40) Mulliken, R. S. Electronic Population Analysis on LCAO−MO Molecular Wave Functions. I. *J. Chem. Phys.* **1955**, *23*, 1833−1840.

(41) Hansch, C.; Leo, A.; Taft, R. W. A Survey of Hammett Substituent Constants and Resonance and Field Parameters. *Chem. Rev.* **1991**, *91*, 165−195.